ISSN 0915-633X

NATIONAL INSTITUTE FOR FUSION SCIENCE

Cooling Effect of Secondary Electrons in the High Temperature Divertor Operation

W.X. Wang, M. Okamoto, N. Nakajima,
S Murakami and N. Ohyabu

(Received - Dec. 12, 1996)

NIFS-480 Feb. 1997

RESEARCH REPORT
NIFS Series

NAGOYA, JAPAN

Cooling Effect of Secondary Electrons in the High Temperature Divertor Operation

W. X. WANG[†], M. OKAMOTO[†,‡], N. NAKAJIMA [†,‡],
S. MURAKAMI[†,‡], N. OHYABU[†,‡]

[†]Department of Fusion Science, The Graduate University for Advanced Studies.

Nagoya 464-01, Japan

[‡]National Institute for Fusion Science,

Nagoya 464-01, Japan

Abstract

The scrape-off layer (SOL) plasma is studied over a wide range of Coulomb collisionality via particle Monte Carlo simulation with focus on the cooling effect of secondary electrons in the high temperature divertor operation. Electron distribution function in collisionless regime shows a large departure from Maxwellian. In the presence of strong secondary electron emission the electron sheath energy transmission factor in collisionless regime is found to be significantly smaller than that of collisional regime. which indicates a higher temperature obtainable in collisionless SOL plasma. In both collisional and collisionless SOL plasma, the change in the conductive energy flux from the core region into the SOL has little influence on the normalized potential drop and electron energy transmission factor, while the electron temperature is raised as the conductive energy flux increases.

Keywords: high temperature divertor operation, secondary electron emission, sheath, Monte Carlo simulation

1. INTRODUCTION

Importance of the divertor plasma study has been emphasized in the recent fusion programs since the divertor is the key ingredient in enhancing the plasma quality as well as handing the high heat flux in future reactor grade devices.

In the conventional divertor scenario such as in the ITER design[1,2], strong temperature and density gradients develop in the scrape-off layer (SOL) plasma along the magnetic field lines. This, in turn. creates a cold, dense radiative plasma near the divertor target and a relatively high temperature and low density plasma surrounding the core plasma. The low temperature plasma in contact with the divertor target reduces plate sputtering and the high temperature of the SOL plasma in contact with the main plasma seems to be required for H-mode. Such an edge plasma condition allows simultaneous achievement of the radiative cooling and H-mode, as seen in DIII-D[3] and ASDEX-U[4]. It is one of the major issues of the ITER design whether such a divertor scenario is operable in the ITER device that definitely satisfies both reduction of the heat load through the radiative cooling and enhancement of the energy confinement. In the conventional divertor operation, the plasma in the SOL region is highly collisional, i.e, the particle Coulomb mean-free-path λ is much less than the parallel dimension L of the SOL.

Recently, a new divertor operational scenario, high temperature divertor plasma operation, has been proposed to enhance the energy confinement in helical devices as well as tokamaks[5,6]. In this approach, a very high temperature of the divertor plasma is maintained by avoiding particle recycling as much as possible. This is accomplished by efficient pumping in the divertor. When the edge temperature exceeds a value seen at the H-mode pedestal, i.e, 300-1000 eV, it can be expected that core energy confinement improves similarly as the formation of the high temperature pedestal leads to the core confinement enhancement in tokamak H-mode discharges. The validity of this concept has been partly demonstrated by recent JT60-U discharges with low recycling, in which ion temperature of the SOL plasma is raised to several keV and a record high value of $n\tau_E T$ (with standard meaning) has been achieved[7]. The high temperature is obtained by using strong pumping under the boron coated wall condition. This type of operation is planned to be pursued further in the LHD device, a large superconducting helical device under construction in Japan[8]. For reactor grade devices, the divertor field lines are needed to be guided into remote chambers outside of the coil cage, where the magnetic

field is weak and large divertor channel is available, thereby reliable heat removal and efficient pumping can be achievable. For heliotron typed helical devices, such a divertor magnetic configuration can be formed easily by a proper arrangement of the coils[9]. In contrast to the conventional divertor operation, the SOL plasma is collisionless in the high temperature divertor operation, namely, $\lambda \gg L$.

In the high temperature divertor operation, one of the key physics issues is influence of the secondary electrons emitted from the divertor plates, which tend to cool the SOL plasma. Maintaining a high edge temperature is critical to achieve the improvement of the energy confinement. Since particle recycling is controlled to be a low level by efficient pumping, the cooling due to atomic processes associated with the particle recycling is not significant. On the other hand, secondary electrons emitted from the plates due to the impact of plasma on the target are inevitable. The secondary electrons are created with smaller initial kinetic energy of a few eV, and become an essential cooling source for the divertor and SOL plasma. To answer the feasibility of the high temperature divertor operation, the influence of secondary electrons on a collisionless SOL plasma should be clarified.

The SOL plasma can be operated over a wide range of Coulomb collisionality. The quantity which measures the collisionality of the SOL system is defined as the ratio of $L/2$ to the particle mean-free path in the parallel direction λ_a, i.e, $L/(2\lambda_a)$, where $\lambda_a = \tau_{aa}\sqrt{2T_{a\|}/m_a}$ (τ_{aa} is the like-particle equilibration time[10] and $T_{a\|}$ is the parallel temperature). The collisionality can range from an extremely small value to a very large value in different operation modes. The distribution function of the SOL plasma, especially in high temperature operation mode, may significantly deviate from Maxwellian. In many previous studies of the SOL plasma, electrons are assumed to be Maxwellian, and only ions are solved. In collisionless SOL plasma of the high temperature operation, however, the assumption of Maxwellian electrons is no more valid. The low collisionality and non-Maxwellian features can significantly affect the transport properties of the SOL plasma. To understand a collisionless SOL plasma, a kinetic treatment for electrons is needed. Since the SOL plasma can be operated from collisional regime to collisionless regime, its dependence on the collisionality should be investigated.

A particle Monte Carlo model with a kinetic treatment for electrons has been developed to study global features of the SOL plasma in connection with main plasma parameters[11].

The global features of the SOL plasma such as temperature, density, total potential drop, etc, are determined consistently with particle and energy flows from the confinement region to the SOL. In this paper, by using the model, we numerically investigate the characteristics of the SOL plasma such as potential formation, effects of secondary electron emission. dependence on collisionality, sheath energy transmission factor, etc. The simulations have been performed over a wide range of Coulomb collisionality with focus on the cooling effect of secondary electrons in collisionless regime, which is importantly relevant to the high temperature divertor operation. A brief description of the Monte Carlo model is given in Section 2. The results of our simulation are presented in Section 3. The conclusions are summarized in Section 4.

2. SIMULATION MODEL

Recently, we have developed a Monte Carlo model with a kinetic treatment on electrons to study global features of the SOL plasma in connection with main plasma parameters[11]. We concentrate on the SOL region between two potential sheaths formed in front of the two divertor plates. In the high temperature divertor operation, the gradient of plasma along the flow direction is not significant in the SOL due to the fast streaming of particles along magnetic field lines. This situation also holds for the SOL defined by a limiter. Assuming that the plasma in the SOL is uniform due to the fast streaming, we have proposed model Fokker-Planck equations for both electrons and ions of the SOL, taking essential physics processes into account[11]. The distribution function of a-species $f_a(\vec{v},t)$ evolves only in velocity space as follows

$$\frac{\partial f_a(\vec{v},t)}{\partial t} = C_a + \text{sources/sinks}, \tag{1}$$

where C_a is Coulomb collision operator. The cross-field plasma transport from the core into the SOL and secondary electron emission from the plates are treated as sources, and particle and energy sink effects due to the absorbing plates are effectively modeled through the connection length L between two divertor plates. In the source terms, the conductive energy flux from the confinement region into the SOL is effectively modeled via randomly exchanging the source particles for the SOL particles. The conductive energy flux, which is independent of cross-field particle flux in determining the SOL structure, together with the convective energy flux introduced by the particle source term, ensures integrated balance

of energy flowing to the SOL and energy lost to the divertor plates. Coulomb collisions are incorporated by a nonlinear Monte Carlo operator[12]. The Coulomb collision effects can be accurately simulated even when the SOL plasma deviates far from a Maxwellian distribution. Instead of solving Possion's equation, the total potential drop between the SOL plasma and the plate is consistently determined by employing the constraint of charge neutrality and the condition of zero-current to the plate. The source and sink terms in Eq.(1) are next explained in detail.

The particle source term $S_{pa}(\vec{v})$ of a-species, used to model the cross-field particle flux from the core region across the separatrix into the SOL is given by

$$S_{pa} = \dot{S}_a \frac{\exp(-m_a v^2/2T_{sa})}{\int \exp(-m_a v^2/2T_{sa}) d^3v}. \tag{2}$$

with T_{sa} defined as source temperature which may be considered as the main plasma temperature very near the separatrix. The source strength $\dot{S}_a$ relates to the total particle flux across the separatrix Γ_a^t as follows

$$\Gamma_a^t \equiv \int_{S_A} \vec{\Gamma}_a \cdot d\vec{S} = \int_{V_{SOL}} d^3x \int d^3v S_{pa} = V_{SOL} \dot{S}_a, \tag{3}$$

where $\vec{\Gamma}_a$ is the particle flux and $\int_{V_{SOL}} d^3x$ is the space integration over the whole SOL volume V_{SOL}. $\dot{S}_a$ is specified via Eq.(3) assuming that Γ_a^t and V_{SOL} are known.

The target plates absorb the particles incident on them along the open magnetic field lines and therefore act as the strong sink for particles and energy in the SOL. The sink effects are described in Eq.(1) by loss terms

$$L_e = -\frac{f_e}{\tau_{\|e}} H(|\vec{v}_\|| - v_c) \tag{4}$$

for electrons and

$$L_i = -\frac{f_i}{\tau_{\|i}} \tag{5}$$

for ions, where the Heaviside step function $H(|\vec{v}_\|| - v_c)$ represents the fact that only untrapped electrons with $v_\| > v_c$ ($v_c = \sqrt{-2e\Phi/m_e}$) can cross the sheath potential barriers (with a height of $-\Phi$, $\Phi < 0$) onto the target plates, and $\tau_{\|a}$ is the particle lifetime defined as the transit time along the magnetic field line to the plates, i.e,

$$\tau_{\|e} = \begin{cases} \infty, & \text{for trapped electrons} \quad \left(v_\| \le v_c\right) \\ \dfrac{L}{2v_\|}, & \text{for untrapped electrons} \quad \left(v_\| > v_c\right) \end{cases}$$

$$\tau_{\|i} = \frac{L}{2v_\|}, \qquad \text{for all ions (untrapped)}$$

The cross-field energy transport from the core region across the separatrix into the SOL includes the contribution from both convective and conductive processes. The convective part is introduced by the particle source term S_{pa}. The conductive part is modeled by the heat source term taken as

$$S_{qa} = \dot{S}_{qa} \left(\frac{\exp\left(-m_a v^2/2T_{sa}\right)}{\int \exp\left(-m_a v^2/2T_{sa}\right) d^3v} - \frac{f_a}{\int f_a d^3v} \right). \tag{6}$$

It introduces a conductive energy flux into the SOL by randomly exchanging the source particles in the confinement region for the SOL particles according to the rate $\dot{S_{qa}}$.

The impact of plasma on the target plates gives rise to the emission of secondary electrons. The influence of secondary electrons is an important issue to be investigated in the high temperature divertor operation. The secondary electron emission term in the model Fokker-Planck equation is expressed as

$$S_{2e} = \delta_e \int \frac{f_e}{\tau_{\|e}} H(|\vec{v}_{\|}| - v_c) d^3v \cdot \frac{g(\vec{v})}{\int g(\vec{v}) d^3v}. \tag{7}$$

where δ_e is the emission coefficient which depends on the energy of incident electrons and the material of the target plate. Secondary electrons are born at the plates with a typical kinetic energy of a few eV and accelerated by the sheath potential to a speed $v_c = \sqrt{-2e\Phi/m_e}$ in entering the SOL (note that magnetic field normal to the plates is assumed). The velocity distribution function $g(\vec{v})$ for secondary electrons as a source in Eq.(7), can be reasonably set as

$$g(\vec{v}) = \exp\left(-\frac{m_e v_\perp^2}{2T_{2e\perp}}\right) \frac{\delta(v_\| - v_c) + \delta(v_\| + v_c)}{2} \tag{8}$$

with $T_{2e\perp} \sim$ a few eV. In Eq.(8), two $\delta-$functions represent two components of the secondary electrons from two divertor plates (or two sides of a limiter), and the perpendicular component is trivially assumed to be Maxwellian.

The model Fokker-Planck equations are solved via particle Monte Carlo simulation. In each time step Δt following the evolution of simulation system, the procedures are as follows:

1. Colliding particles with each other, which changes particle velocities via the Monte Carlo nonlinear collision operator;

2. Removing some particles from the system according to the sink terms in the equations, which models the loss of particles and energy to the plates;

3. Replacing randomly some particles with the source particles (i.e., the main plasma near the separatrix) in terms of S_{qe} and S_{qi}, which models the cross-field conductive heat flux from the core region;

4. Injecting new particles into the system in terms of S_{pe}, S_{pi} and S_{2e}, which models the ambipolar cross-field particle transport from the core region and the secondary electron emission from the plates, respectively.

The step 2 is incorporated via killing particles. The probability of a particle to be killed in a time interval Δt is

$$p(v_{\|}) = \begin{cases} 1 - e^{-\frac{\Delta t}{\tau_{\|a}(v_{\|})}}, & \text{for untrapped electrons } (v_{\|} > v_c) \text{ and ions} \\ 0. & \text{otherwise.} \end{cases}$$

Whether a particle is killed is determined by comparing $p(v_{\|})$ with a random number uniformly distributed between 0 and 1. Time is advanced by repeating steps 1-4 until the system becomes stationary satisfying the charge neutrality and zero-current condition. A steady state SOL plasma and total potential drop are finally obtained in terms of total particle flux and input power across the separatrix, the temperature of main plasma near the separatrix, secondary electron emission coefficient, and the SOL size.

3. SIMULATION RESULTS

The SOL plasma is simulated by the above model over a wide range of Coulomb collisionality. We neglect electron-ion collisions for numerical simplicity. The ramifications of neglecting unlike collisions were previously discussed[11]. The input parameters are listed in Table I. The collisionality is changed by varying the connection length L. The secondary electron emission coefficient δ_e takes 0.0, 0.5 and 0.8 in the simulations.

TABLE I. PARAMETERS USED TO SIMULATE SOL PLASMA

Total particle fluxes	$\Gamma_e^t = \Gamma_i^t = 6.0 \times 10^{21}$ sec^{-1}
Source temperatures	$T_{se} = T_{si} = T_s = 2.0$ keV
SOL volume	$V_{SOL} = 0.5$ m^3
Electron exchange rate	$\dot{S}_{qe} = 1.0 \sim 7.0\dot{S}_i$
	$(\dot{S}_i = \dot{S}_e = \Gamma_i^t / V_{SOL}$
	$= 1.2 \times 10^{22}$ m^{-3}sec^{-1})
Ion exchange rate	$\dot{S}_{qi} = 0.0$
Secondary electron emission coefficient	$\delta_e = 0.0,\ 0.5,\ 0.8$
Perpendicular temperature of secondary electrons	$T_{2e\perp} = 1.0$ eV
Mass ratio	$m_i/m_e = 1836$ (hydrogen)
Magnetic field line length	$L = \begin{cases} 2450.0 \text{ m}, & \text{collisional} \\ 590.1 \text{ m}, & \text{moderate} \\ 122.5 \text{ m}, & \text{collisionless} \end{cases}$

Figure 1 shows the dependence of the ion density (i.e, plasma density) of the SOL plasma on the the connection length L. Because the strength of the plate sink action is inversely dependent on the connection length (see Eqs.(4) and (5)), the plasma density of the SOL increases as the connection length increases. In Fig.1, $\log(n_i/n_s)$ and $\log(L/2\tau_s v_s)$ obey following linear relation approximately

$$\log \frac{n_i}{n_s} = 1.80 + 0.827 \log(\frac{L}{2\tau_s v_s}) \tag{9}$$

within the accuracy of 3%, where $v_s = \sqrt{2T_s/m_e}$ and time scale τ_s and density scale n_s used for normalization are defined by the relations

$$\dot{S}_i = \frac{n_s}{\tau_s} \quad \text{and} \quad \tau_s = \frac{3\sqrt{m_e}T_s^{3/2}}{4\sqrt{\pi}e^4 n_s \ln\Lambda}.$$

The Coulomb logarithm is set to be a constant ($\ln\Lambda = 17$) in the simulations.

It was shown by the previous simulation that the electron distribution function in the collisional SOL plasma ($L = 2450$ m) is nearly Maxwellian[11]. In collisionless SOL plasma the situation is very different. Figure 2 shows the steady-state electron distribution function of collisionless SOL plasma in the simulation with $L = 122.5$ m and $\delta_e = 0.8$. The parallel distribution function (Fig.2(a)) shows truncated tails outside $v_{||} = v_c$ because

energetic electrons with $\frac{1}{2}m_e v_\parallel^2 > -e\Phi$ are directly lost and the collisions are too weak to supply sufficient electrons into the loss region with $v_\parallel > v_c$. Also due to the low collisionality secondary electrons are not thermalized, as is indicated by the peaks near $v_\parallel = v_c$ in Fig.2(a) as well as the small contours near $v_\parallel = v_c$ in Fig.2(b). Compared to the circular contour plot of electron distribution in collisional case[11], the contour plot in Fig.2(b) indicates that electron are anisotropic in collisionless case. In many previous studies a Maxwellian distribution is assumed for electrons. However, as seen from Fig.2, the electron distribution function is far from a Maxwellian in low collisionality regime, which also indicates that, in studying the SOL plasma a kinetic treatment for electrons is required and a nonlinear collision operator should be used.

The conductive energy flux from the confinement region into the SOL has been included in the model in addition to the convective energy flux to ensure integrated balance of energy flowing to the SOL and energy lost to the limiter/divertor plates. The conductive energy flux can not be neglected in a self-consistent determination of the SOL structure. The influence of conductive energy flux on the SOL plasma is now examined by changing the conductive input power through the exchange rate $\dot{S}_{qe}$. The conductive input power is contributed by cross-field conductive energy flux $\vec{q}_e^{\,cond}$ of electron

$$Q_e^{cond} \equiv \int_{S_A} \vec{q}_e^{\,cond} \cdot \vec{S} = \frac{3}{2}\dot{S}_{qe}(T_{se} - T_e), \tag{10}$$

where integration is performed over the separatrix surface S_A. The simulations are performed for collisional ($L = 2450$ m) and collisionless ($L = 122.5$ m) SOL plasma with the secondary electron emission coefficient $\delta_e = 0.5$. The variations of normalized total potential drop $e\Phi/T_{e\parallel}$, electron sheath energy transmission factor γ_e and electron temperature with conductive input power Q_e^{cond} are illustrated in Fig.3. The electron energy transmission factor is defined as

$$P_e = \gamma_e T_e \Gamma_i^{loss}. \tag{11}$$

where P_e is electron loss energy flux of the SOL to the plate, T_e is the electron temperature of the SOL and Γ_i^{loss} is ion loss flux to the plate, which is equal to net electron flux to the plate. Figures 3(a) and 3(b) show that the conductive energy flux has little influence on $e\Phi/T_{e\parallel}$ and γ_e in both collisional and collisionless SOL plasmas. While the electron temperature shown in Fig.3(c) sensitively depends on the conductive energy flux. The electron temperature rises as the conductive input power is increased. As discussed previously, the energy exchange between electrons and ions due to e-i collisions is weak

even in a collisional SOL plasma[11]. As energy exchange between electrons and ions is neglected, Eq.(11) can be rewritten at steady state as

$$Q_e^{in} = \gamma_e T_e \Gamma_i^{t,loss}, \tag{12}$$

where Q_e^{in} is the total electron input power across separatrix into the SOL and $\Gamma_i^{t,loss}$ is total ion loss flux to the plates (i.e, the flux integrated over the surface of the plates). The total electron input power Q_e^{in} consists of the conductive input power Q_e^{cond} and the convective input power Q_e^{conv}. Since the total input flux Γ_e^t is fixed, the total loss flux $\Gamma_i^{t,loss}$ and the convective input power Q_e^{conv} are fixed. With regard to the energy balance relation given by Eq.(12), the results shown in Figs.3(b) and 3(c) state that the change in Q_e^{in} only due to the conductive input power Q_e^{cond} causes the essential change in the electron temperature T_e but not in the electron energy transmission factor γ_e. The electron temperature T_e increases with proportional to the conductive input power Q_e^{cond} under the fixed collisionality. In contrast with it, the electron energy transmission factor γ_e is almost independent of the conductive input power Q_e^{cond}, but depends on the collisionality. Although it is difficult to control Q_e^{in} in a simulation (note that Q_e^{cond} is not a direct input parameter as is seen from Eq.(10)), it is possible to compare various simulation results with different collisionality under the same total electron input power by utilizing the fact that the electron energy transmission factor γ_e is almost independent of the conductive input power Q_e^{cond}. Namely, under the same total electron input power and the different collisionalities, the electron temperature at the steady state T_e is inversely proportional to the electron energy transmission factor γ_e; $T_e \propto 1/\gamma_e$.

The isothermal fluid model[13] gives normalized potential drop $e\Phi/T_e$ and electron sheath energy transmission factor γ_e as follows

$$\frac{e\Phi}{T_e} = \frac{1}{2}\ln[(2\pi\frac{m_e}{m_i})(1+\frac{T_i}{T_e})(1-\delta_e)^{-2}] - \ln(2-\frac{V_0}{c_s}), \tag{13}$$

$$\gamma_e = \frac{2}{1-\delta_e} - \frac{e\Phi}{T_e}, \tag{14}$$

where V_0 and c_s are the ion initial mean speed (the speed at the point far from the plasma-sheath interface) and the ion acoustic speed, respectively. Our simulation results of $e\Phi/T_e$ and γ_e for collisional SOL plasma have been shown to be in close agreement with these analytic predictions[11]. The simulations are performed over a wide range of collisionality. The dependences of $e\Phi/T_{e\|}$ and γ_e on collisionality are presented in Fig.4.

Note that in these simulations, the cross-field particle flux and then cross-field convective energy flux of electrons are same (i.e, $\dot{S}_e$ is same), but the conductive energy flux and then conductive input power of electrons are different. Since, as indicated in Fig.3, the normalized potential drop $e\Phi/T_{e\|}$ and electron energy transmission factor are not sensitive to the conductive input power, the difference in $e\Phi/T_{e\|}$ shown in Fig.4(a) and difference in γ_e shown in Fig.4(b) are attributed essentially to the difference in collisionality and in secondary electron emission coefficient. In Fig.4(a), increase in the secondary emission coefficient is found, over a wide range of collisionality, to reduce the total potential drop. This observation can be understood from the condition of zero-current to the plate

$$\Gamma_i^{loss} = \Gamma_e^{loss} = (1 - \delta_e)\Gamma_{e0}^{loss}, \tag{15}$$

where Γ_e^{loss} and Γ_{e0}^{loss} are electron net loss flux and primary electron loss flux to the plate, respectively. As the secondary emission is increased, the primary electron flux must increase to maintain a constant net flux and then a zero current to the plate. This is done by reducing the potential drop to enlarge the number of untrapped electrons, as indicated by Fig.4(a). For the same secondary emission coefficient, the normalized potential drop $e\Phi/T_{e\|}$ in Fig.4(a) shows an increase with collisionality, which is consistent with the results of PIC simulations[14,15] where the secondary emission is not included. To understand the increase of $e\Phi/T_{e\|}$ with collisionality, it is helpful to compare the parallel electrons distribution function in collisionless case (see Fig.2(a)) to that in collisional case which is close to a Maxwellian[11]. The parallel distribution function in collisionless SOL plasma has a truncated tail outside $v_{\|} > v_c$. The primary electron flux to the plate is contributed only by the tail with $v_{\|} > v_c$ of the distribution function. For a collisionless SOL plasma having the same primary electron flux to the plate as collisional SOL plasma, a lower potential barrier is needed. Thus, the potential drop increases with collisionality as shown in Fig.4(a). It is also shown in Fig.4(a) that the increase in $e\Phi/T_{e\|}$ becomes slower as the the secondary emission becomes stronger.

The analytical prediction of γ_e, Eq.(14), is based on the hydrodynamic description of ions and the assumption of Maxwellian electrons, and thus not valid for collisionless SOL plasma. In Fig.4(b), for the same secondary emission coefficient the electron energy transmission factor γ_e is found to decrease with the decrease in collisionality. Especially in the presence of strong secondary emission, γ_e in low collisionality regime is significantly reduced relative to the one in high collisionality regime. This result provided by our

simulations is essential for us to understand the cooling effect of secondary electrons in the high temperature divertor operation. The cooling role of secondary electrons occurs in whole collisionality regime, which can be seen in Fig.4(b) where γ_e increases with δ_e over a wide range of collisionality. The secondary electrons cool the SOL plasma partially through reducing the sheath potential and partially through collisional energy exchange. As is mentioned in the previous paragraph with regard to EQ.(11), we know that, with the same input power, the electron temperature at the steady state is decreased as the secondary emission increases. The smaller values of γ_e shown in Fig.4(b) mean higher temperatures T_e in collisionless SOL than in collisional SOL (under the same input power). Since γ_e is reduced with the decrease in the collisionality, the cooling effect of secondary electrons becomes weak in collisionless case. Therefore, even if there is a strong secondary emission, the high temperature can be maintained in the collisionless SOL plasma.

4. SUMMARY

The SOL plasma has been simulated over a wide range of collisionality by using the particle Monte Carlo model.

The collisionless SOL plasma has been investigated related to the high temperature divertor operation. A strong deviation of the electron distribution function from Maxwellian has been shown. The low collisionality and non-Maxwellian features affect the transport properties of the SOL plasma, and result in the total potential drop and electron energy transmission factor differing significantly from the analytical estimates. It has been found that γ_e is reduced as decreasing collisionality and that its value in collisionless regime is considerably smaller than in collisional regime. This fact indicates that the SOL plasma is not cooled by secondary electrons in collisionless case because the electron equilibrium temperature is inversely proportional to γ_e. The numerical study here provides a primary understanding of cooling effect of secondary electrons in the high temperature divertor operation and a positive evidence that the high temperature divertor operation may be possible.

The influence of cross-field conductive energy flux on the SOL plasma has been investigated. $e\Phi/T_{e\|}$ and γ_e are found to be insensitive to the change in the electron conductive input power; while T_e is raised as the conductive input power increases.

Our simulations have also demonstrated that the potential drop $-e\Phi/T_{e\|}$ increases

with collisionality and decreases with increasing the secondary emission.

ACKNOWLEDGMENTS

One of the authors (W. X. Wang) would like to acknowledge hospitality of the Theory and Data Analysis Division of The National Institute for Fusion Science (NIFS). He also thanks professor T. Q. Chang for his support and encouragement. Numerical calculations were carried out by using the super computer SX-3 of NIFS.

REFERENCES

[1] D. E. Post, in Plasma Physics and Controlled Nuclear Fusion Research 1988 (Proc. 12th Int. Conf. Nice, 1988), Vol. 3, IAEA, Vienna (1989) 233.

[2] W. L. Barr, Summary of Ways to Reduce the Divertor Heat Load and Erosion in ITER, ITER Memo LLNL-ITER-88-036, Lawrence Livermore National Laboratory, Livermore, CA (1988).

[3] LUXON, J., et al., in Plasma Physics and Controlled Nuclear Fusion Research 1986 (Proc. 11th Int. Conf. Kyoto, 1986), Vol. 1, IAEA, Vienna (1987) 159.

[4] WAGNER, F., et al., Phys. Rev. Lett. **49**, (1982) 1048.

[5] OHYABU, N., et al., in Plasma Physics and Controlled Nuclear Fusion Research 1992 (Proc. 14th Int. Conf. Würzburg. 1992), Vol. 2, IAEA, Vienna (1993) 605.

[6] OHYABU, N., et al., Nucl. Fusion **34** (1994) 387.

[7] KONOSHIMA, S., TOI, K., J. Plasma and Fusion Res. **71** (1995) 109.

[8] IIYOSHI, A., Fusion Technol. **17** (1990) 169.

[9] TAKASE, H., OHYABU, N., Nucl. Fusion **35** (1995) 123.

[10] HINTON, F.L., in Handbook of Plasma Physics (ROSENBLUTH, M.N., SAGDEEV, R.Z., Ed.), Vol. 1, North-Holland Publishing Company, Amsterdam (1983) 147.

[11] WANG, W.X., et al., A Monte Carlo Model for Velocity Space Effects in Low Recycling Scrape-off Layer Plasmas, to be published in Nucl. Fusion.

[12] WANG, W.X., et al., J. Comput. Phys. **128** (1996) 209.

[13] STANGEBY, P.C., Phys. Fluids **27** (1984) 682.

[14] PROCASSINI, R.J., BIRDSALL, C.K., Phys. Fluids B **3** (1991) 1876.

[15] PROCASSINI, R.J., et al., Nucl. Fusion **30** (1990) 2329.

Figure Captions

Fig. 1 Dependence of the SOL plasma density on the connection length L.

Fig. 2 Electron distribution function from the simulation of collisionless SOL plasma with $\delta_e = 0.8$: (a) parallel distribution function $\log f_{e\|}$ vs. $m_e v_\|^2/(2T_{e\|})$ (the dashed line shows the Maxwellian distribution with the same temperature and the dotted lines denote the positions of $v_\| = v_c \equiv \sqrt{-2e\Phi/m_e}$.) and (b) contour plot of the distribution function (velocities are normalized by the thermal velocity of source $v_s = \sqrt{2T_s/m_e}$).

Fig. 3 Dependence of (a) normalized potential $-e\Phi/T_{e\|}$, (b) electron energy transmission factor γ_e and (c) electron temperature T_e on the conductive input power Q_e^{cond} for both collisional (circles) and collisionless (squares) SOL plasma.

Fig. 4 Dependence of (a) the normalized potential $-e\Phi/T_{e\|}$ and (b) the electron energy transmission factor γ_e on Coulomb collisionality for three secondary emission coefficients, $\delta_e = 0$ (circles), $\delta_e = 0.5$ (squares) and $\delta_e = 0.8$ (triangles).

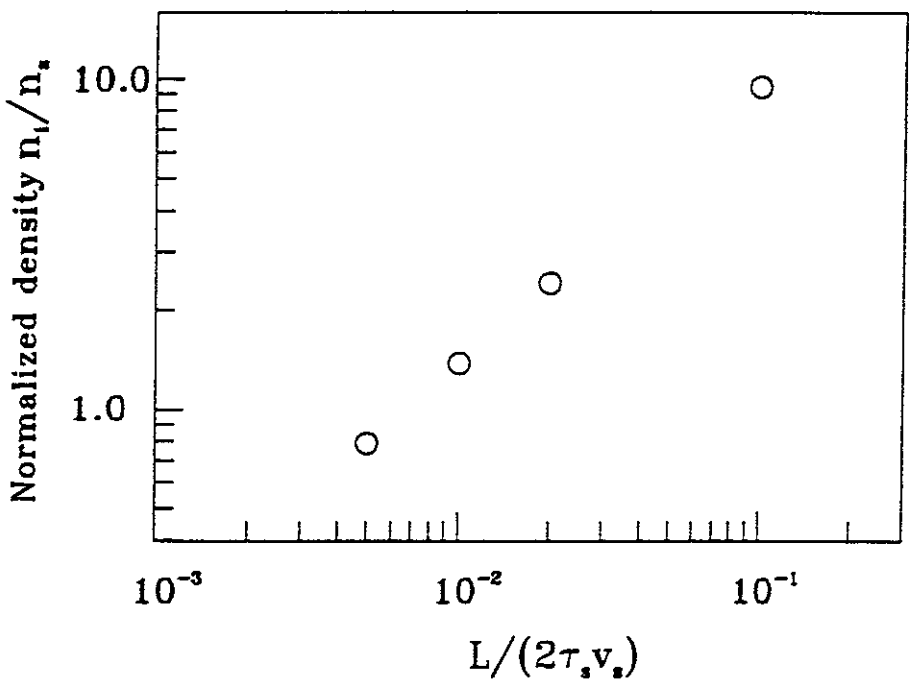

Fig. 1 *Dependence of the SOL plasma density on the connection length L.*

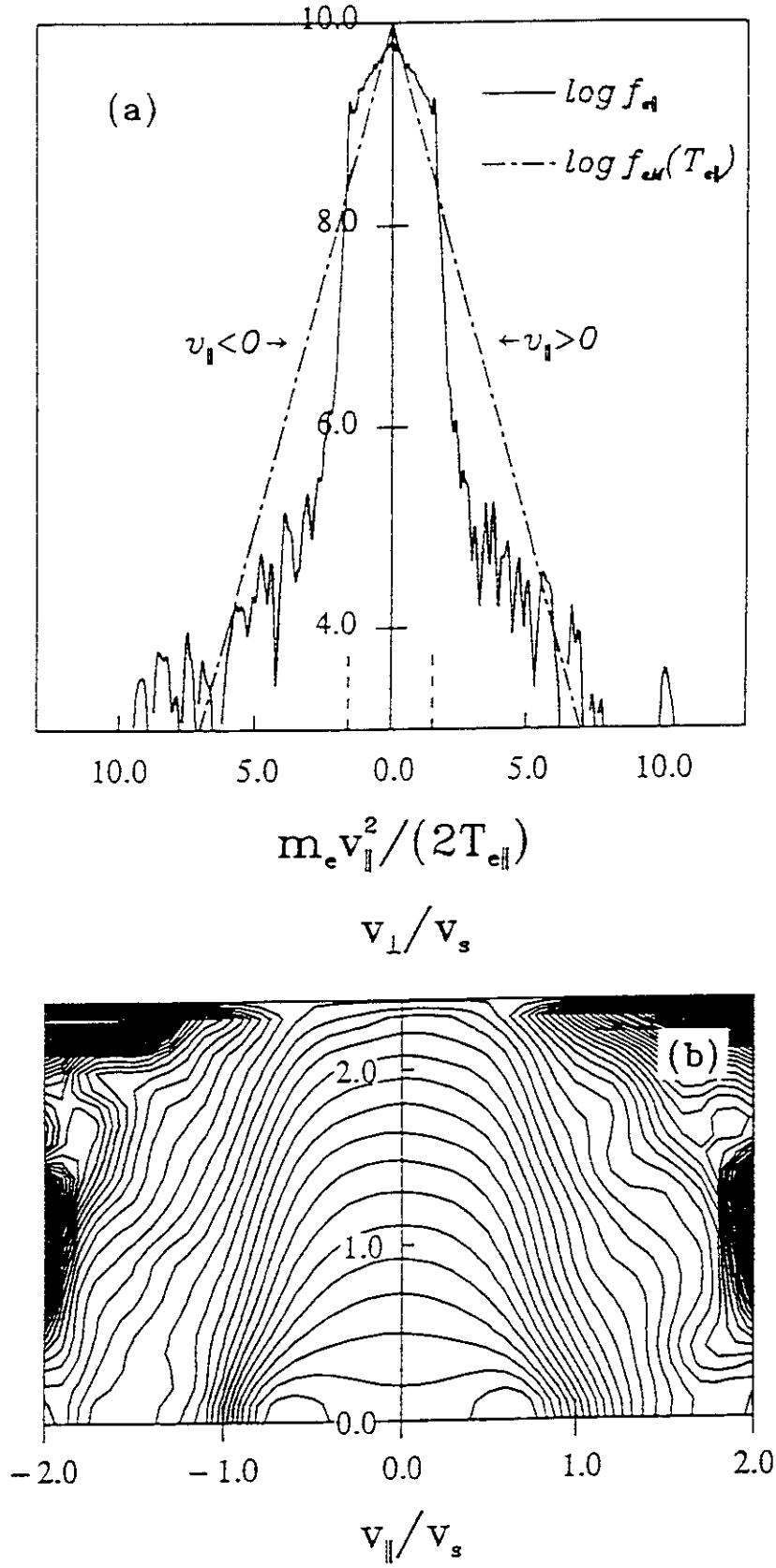

Fig. 2 *Electron distribution function from the simulation of collisionless SOL plasma with* $\delta_e = 0.8$*: (a) parallel distribution function* $\log f_{e\|}$ *vs.* $m_e v_\|^2/(2T_{e\|})$ *(the dashed line shows the Maxwellian distribution with the same temperature and the dotted lines denote the positions of* $|\vec{v_\|}| = v_c \equiv \sqrt{-2e\Phi/m_e}$*) and (b) contour plot of the distribution function (velocities are normalized by the thermal velocity of source* $v_s = \sqrt{2T_s/m_e}$*).*

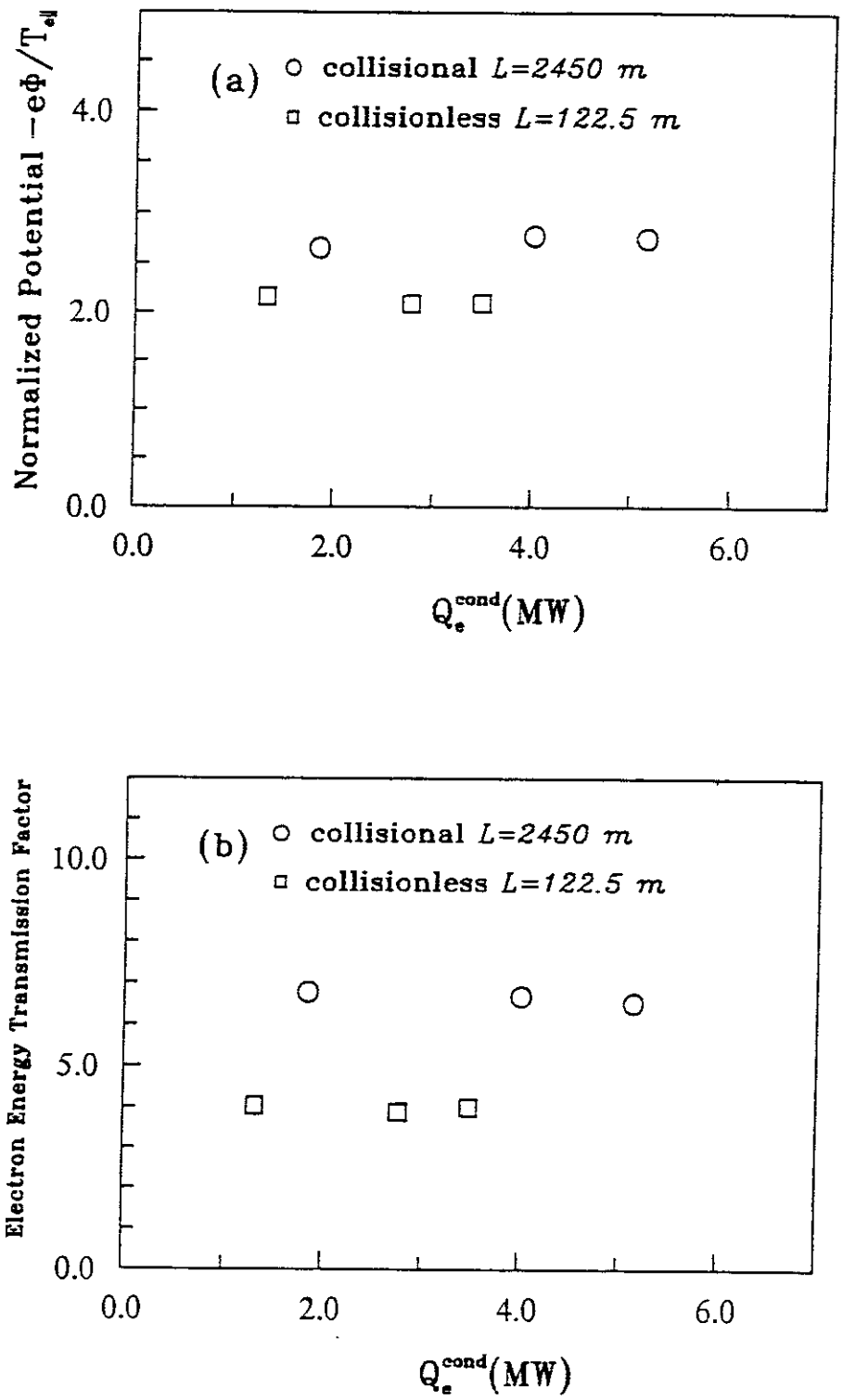

Fig. 3 *Dependence of (a) normalized potential $-e\Phi/T_{e\|}$, (b) electron energy transmission factor γ_e and (c) electron temperature T_e on the conductive input power Q_e^{cond} for both collisional (circles) and collisionless (squares) SOL plasma.*

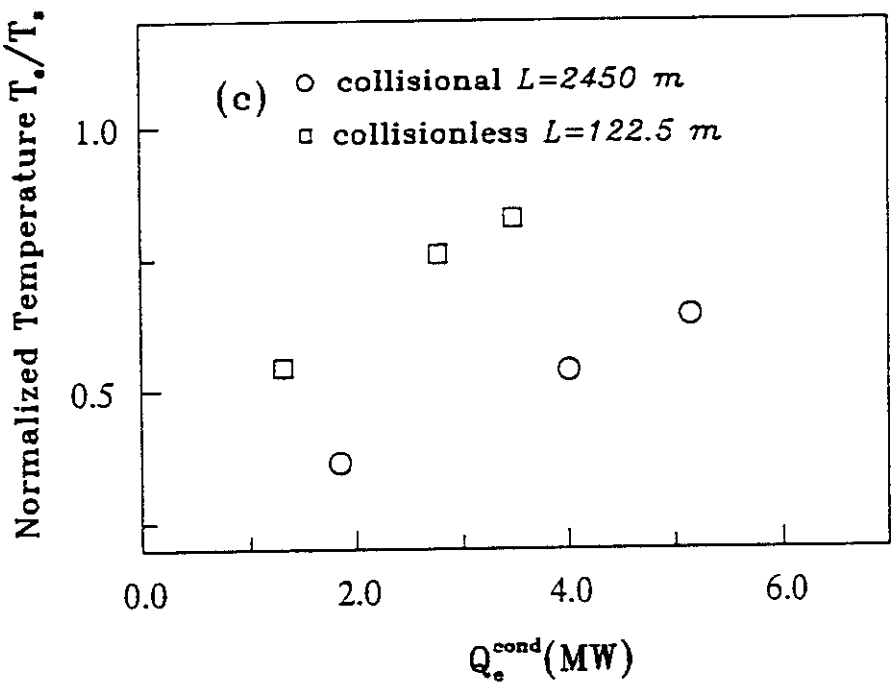
(c)
collisional L=2450 m
collisionless L=122.5 m
Normalized Temperature T_e/T_e
1.0
0.5
0.0
2.0
4.0
6.0
Q_e^{cond}(MW)

Fig. 3(c)

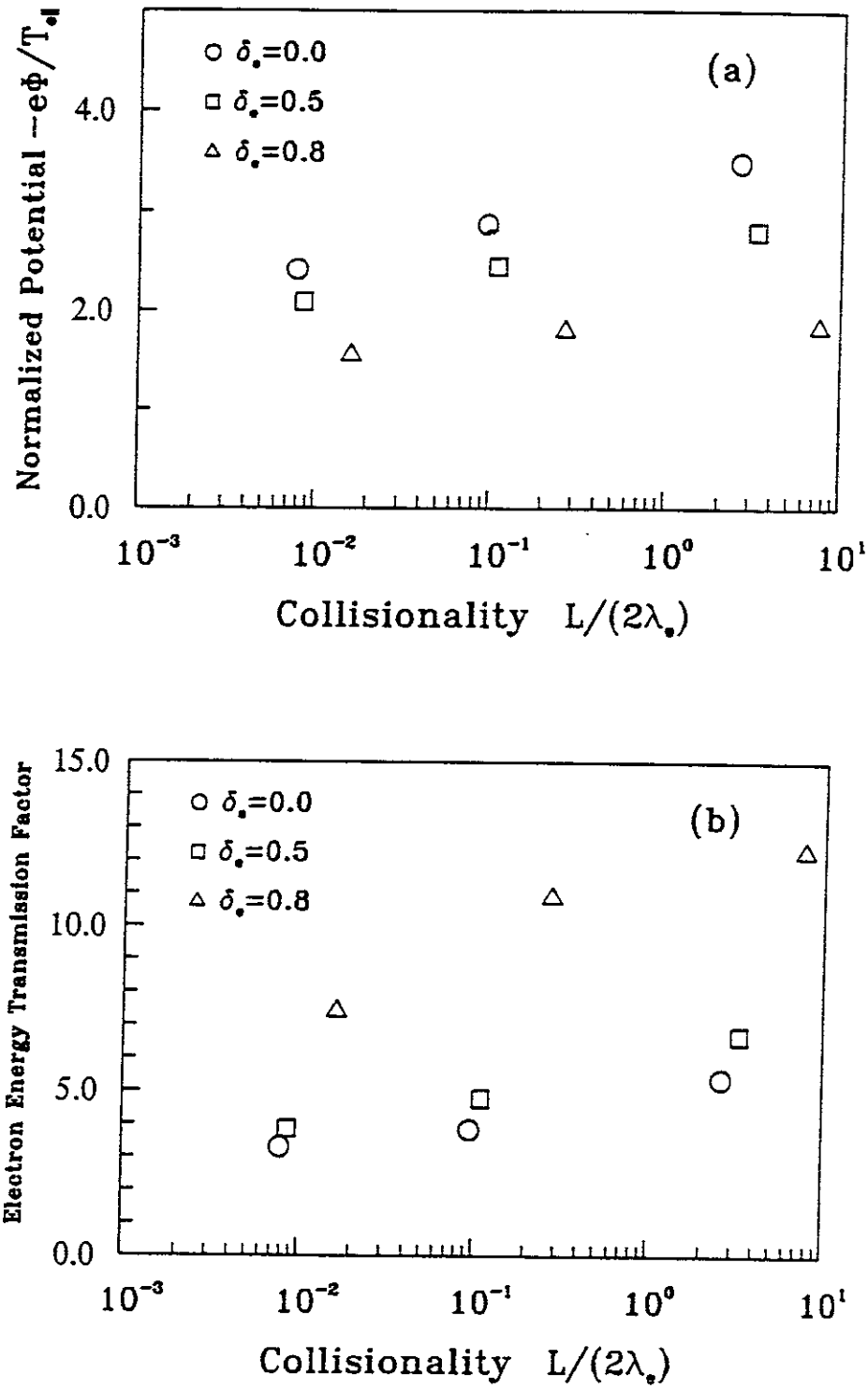

Fig. 4 *Dependence of (a) the normalized potential $-e\Phi/T_{e\|}$ and (b) the electron energy transmission factor γ_e on Coulomb collisionality for three secondary emission coefficients, $\delta_e = 0$ (circles), $\delta_e = 0.5$ (squares) and $\delta_e = 0.8$ (triangles).*

Recent Issues of NIFS Series

NIFS-440 S. Morita, H. Idei, H. Iguchi, S. Kubo, K. Matsuoka, T. Minami, S. Okamura, T. Ozaki, K. Tanaka, K. Toi, R. Akiyama, A. Ejiri, A. Fujisawa, M. Fujiwara, M. Goto, K. Ida, N. Inoue, A. Komori, R. Kumazawa, S. Masuzaki, T. Morisaki, S. Muto, K. Narihara, K. Nishimura, I. Nomura, S. Ohdachi, M.. Osakabe, A. Sagara, Y. Shirai, H. Suzuki, C. Takahashi, K. Tsumori, T. Watari, H. Yamada and I. Yamada,
A Study on Density Profile and Density Limit of NBI Plasmas in CHS; Sep. 1996 (IAEA-CN-64/CP-3)

NIFS-441 O. Kaneko, Y. Takeiri, K. Tsumori, Y. Oka, M. Osakabe, R. Akiyama, T. Kawamoto, E. Asano and T. Kuroda,
Development of Negative-Ion-Based Neutral Beam Injector for the Large Helical Device; Sep. 1996 (IAEA-CN-64/GP-9)

NIFS-442 K. Toi, K.N. Sato, Y. Hamada, S. Ohdachi, H. Sakakita, A. Nishizawa, A. Ejiri, K. Narihara, H. Kuramoto, Y. Kawasumi, S. Kubo, T. Seki, K. Kitachi, J. Xu, K. Ida, K. Kawahata, I. Nomura, K. Adachi, R. Akiyama, A. Fujisawa, J. Fujita, N. Hiraki, S. Hidekuma, S. Hirokura, H. Idei, T. Ido, H. Iguchi, K. Iwasaki, M. Isobe, O. Kaneko, Y. Kano, M. Kojima, J. Koog, R. Kumazawa, T. Kuroda, J. Li, R. Liang, T. Minami, S. Morita, K. Ohkubo, Y. Oka, S. Okajima, M. Osakabe, Y. Sakawa, M. Sasao, K. Sato, T. Shimpo, T. Shoji, H. Sugai, T. Watari, I. Yamada and K. Yamauti,
Studies of Perturbative Plasma Transport, Ice Pellet Ablation and Sawtooth Phenomena in the JIPP T-IIU Tokamak; Sep. 1996 (IAEA-CN-64/A6-5)

NIFS-443 Y. Todo, T. Sato and The Complexity Simulation Group,
Vlasov-MHD and Particle-MHD Simulations of the Toroidal Alfvén Eigenmode; Sep. 1996 (IAEA-CN-64/D2-3)

NIFS-444 A. Fujisawa, S. Kubo, H. Iguchi, H. Idei, T. Minami, H. Sanuki, K. Itoh, S. Okamura, K. Matsuoka, K. Tanaka, S. Lee, M. Kojima, T.P. Crowley, Y. Hamada, M. Iwase, H. Nagasaki, H. Suzuki, N. Inoue, R. Akiyama, M. Osakabe, S. Morita, C. Takahashi, S. Muto, A. Ejiri, K. Ida, S. Nishimura, K. Narihara, I. Yamada, K. Toi, S. Ohdachi, T. Ozaki, A. Komori, K. Nishimura, S. Hidekuma, K. Ohkubo, D.A. Rasmussen, J.B. Wilgen, M. Murakami, T. Watari and M. Fujiwara,
An Experimental Study of Plasma Confinement and Heating Efficiency through the Potential Profile Measurements with a Heavy Ion Beam Probe in the Compact Helical System; Sep. 1996 (IAEA-CN-64/C1-5)

NIFS-445 O. Motojima, N. Yanagi, S. Imagawa, K. Takahata, S. Yamada, A. Iwamoto, H. Chikaraishi, S. Kitagawa, R. Maekawa, S. Masuzaki, T. Mito, T. Morisaki, A. Nishimura, S. Sakakibara, S. Satoh, T. Satow, H. Tamura, S. Tanahashi, K. Watanabe, S. Yamaguchi, J. Yamamoto, M.Fujiwara and A. Iiyoshi,
Superconducting Magnet Design and Construction of LHD; Sep. 1996 (IAEA-CN-64/G2-4)

NIFS-446 S. Murakami, N. Nakajima, S. Okamura, M. Okamoto and U. Gasparino,
Orbit Effects of Energetic Particles on the Reachable β–Value and the Radial

Electric Field in NBI and ECR Heated Heliotron Plasmas; Sep. 1996 (IAEA-CN-64/CP -6) Sep. 1996

NIFS-447 K. Yamazaki, A. Sagara, O. Motojima, M. Fujiwara, T. Amano, H. Chikaraishi, S. Imagawa, T. Muroga, N. Noda, N. Ohyabu, T. Satow, J.F. Wang, K.Y. Watanabe, J. Yamamoto . H. Yamanishi, A. Kohyama, H. Matsui, O. Mitarai, T. Noda. A.A. Shishkin, S. Tanaka and T. Terai
Design Assessment of Heliotron Reactor; Sep. 1996 (IAEA-CN-64/G1-5)

NIFS-448 M. Ozaki, T. Sato and the Complexity Simulation Group,
Interactions of Convecting Magnetic Loops and Arcades; Sep. 1996

NIFS-449 T. Aoki,
Interpolated Differential Operator (IDO) Scheme for Solving Partial Differential Equations; Sep. 1996

NIFS-450 D. Biskamp and T. Sato,
Partial Reconnection in the Sawtooth Collapse; Sep. 1996

NIFS-451 J. Li, X. Gong, L. Luo, F.X. Yin, N. Noda, B. Wan, W. Xu, X. Gao, F. Yin. J.G. Jiang, Z. Wu., J.Y. Zhao, M. Wu, S. Liu and Y. Han,
Effects of High Z Probe on Plasma Behavior in HT-6M Tokamak; Sep. 1996

NIFS-452 N. Nakajima, K. Ichiguchi, M. Okamoto and R.L. Dewar,
Ballooning Modes in Heliotrons/Torsatrons; Sep. 1996 (IAEA-CN-64/D3-6)

NIFS-453 A. Iiyoshi,
Overview of Helical Systems; Sep. 1996 (IAEA-CN-64/O1-7)

NIFS-454 S. Saito, Y. Nomura, K. Hirose and Y.H. Ichikawa,
Separatrix Reconnection and Periodic Orbit Annihilation in the Harper Map; Oct. 1996

NIFS-455 K. Ichiguchi, N. Nakajima and M. Okamoto,
Topics on MHD Equilibrium and Stability in Heliotron / Torsatron; Oct. 1996

NIFS-456 G. Kawahara, S. Kida, M. Tanaka and S. Yanase,
Wrap, Tilt and Stretch of Vorticity Lines around a Strong Straight Vortex Tube in a Simple Shear Flow; Oct. 1996

NIFS-457 K. Itoh, S.- I. Itoh, A. Fukuyama and M. Yagi,
Turbulent Transport and Structural Transition in Confined Plasmas; Oct. 1996

NIFS-458 A. Kageyama and T. Sato,
Generation Mechanism of a Dipole Field by a Magnetohydrodynamic Dynamo; Oct. 1996

NIFS-459 K. Araki, J. Mizushima and S. Yanase,
The Non-axisymmetric Instability of the Wide-Gap Spherical Couette Flow; Oct. 1996

NIFS-460 Y. Hamada, A. Fujisawa, H. Iguchi, A. Nishizawa and Y. Kawasumi,
A Tandem Parallel Plate Analyzer; Nov. 1996

NIFS-461 Y. Hamada, A. Nishizawa, Y. Kawasumi, A. Fujisawa, K. Narihara, K. Ida, A. Ejiri, S. Ohdachi, K. Kawahata, K. Toi, K. Sato, T. Seki, H. Iguchi, K. Adachi, S. Hidekuma, S.Hirokura, K. Iwasaki, T. Ido, M. Kojima, J. Koong, R. Kumazawa, H. Kuramoto, T. Minami, I. Nomura, H. Sakakita, M. Sasao, K.N. Sato, T. Tsuzuki, J. Xu, I. Yamada and T. Watari,
Density Fluctuation in JIPP T-IIU Tokamak Plasmas Measured by a Heavy Ion Beam Probe; Nov. 1996

NIFS-462 N. Katsuragawa, H. Hojo and A. Mase,
Simulation Study on Cross Polarization Scattering of Ultrashort-Pulse Electromagnetic Waves; Nov. 1996

NIFS-463 V. Voitsenya, V. Konovalov, O. Motojima, K. Narihara, M. Becker and B. Schunke,
Evaluations of Different Metals for Manufacturing Mirrors of Thomson Scattering System for the LHD Divertor Plasma; Nov. 1996

NIFS-464 M. Pereyaslavets, M. Sato, T. Shimozuma, Y. Takita, H. Idei, S. Kubo, K. Ohkubo and K. Hayashi,
Development and Simulation of RF Components for High Power Millimeter Wave Gyrotrons; Nov. 1996

NIFS-465 V.S. Voitsenya, S. Masuzaki, O. Motojima, N. Noda and N. Ohyabu,
On the Use of CX Atom Analyzer for Study Characteristics of Ion Component in a LHD Divertor Plasma; Dec. 1996

NIFS-466 H. Miura and S. Kida,
Identification of Tubular Vortices in Complex Flows; Dec. 1996

NIFS-467 Y. Takeiri, Y. Oka, M. Osakabe, K. Tsumori, O. Kaneko, T. Takanashi, E. Asano, T. Kawamoto, R. Akiyama and T. Kuroda,
Suppression of Accelerated Electrons in a High-current Large Negative Ion Source; Dec. 1996

NIFS-468 A. Sagara, Y. Hasegawa, K. Tsuzuki, N. Inoue, H. Suzuki, T. Morisaki, N. Noda, O. Motojima, S. Okamura, K. Matsuoka, R. Akiyama, K. Ida, H. Idei, K. Iwasaki, S. Kubo, T. Minami, S. Morita, K. Narihara, T. Ozaki, K. Sato, C. Takahashi, K. Tanaka, K. Toi and I. Yamada,
Real Time Boronization Experiments in CHS and Scaling for LHD; Dec. 1996

NIFS-469 V.L. Vdovin, T.Watari and A. Fukuyama,
3D Maxwell-Vlasov Boundary Value Problem Solution in Stellarator Geometry in Ion Cyclotron Frequency Range (final report); Dec. 1996

NIFS-470 N. Nakajima, M. Yokoyama, M. Okamoto and J. Nührenberg,
Optimization of M=2 Stellarator; Dec. 1996

NIFS-471 A. Fujisawa, H. Iguchi, S. Lee and Y. Hamada,
Effects of Horizontal Injection Angle Displacements on Energy Measurements with Parallel Plate Energy Analyzer; Dec. 1996

NIFS-472 R. Kanno, N. Nakajima, H. Sugama, M. Okamoto and Y. Ogawa,
Effects of Finite-β and Radial Electric Fields on Neoclassical Transport in the Large Helical Device; Jan. 1997

NIFS-473 S. Murakami, N. Nakajima, U. Gasparino and M. Okamoto,
Simulation Study of Radial Electric Field in CHS and LHD; Jan. 1997

NIFS-474 K. Ohkubo, S. Kubo, H. Idei, M. Sato, T. Shimozuma and Y. Takita,
Coupling of Tilting Gaussian Beam with Hybrid Mode in the Corrugated Waveguide; Jan. 1997

NIFS-475 A. Fujisawa, H. Iguchi, S. Lee and Y. Hamada,
Consideration of Fluctuation in Secondary Beam Intensity of Heavy Ion Beam Prove Measurements; Jan. 1997

NIFS-476 Y. Takeiri, M. Osakabe, Y. Oka, K. Tsumori, O. Kaneko, T. Takanashi, E. Asano, T. Kawamoto, R. Akiyama and T. Kuroda,
Long-pulse Operation of a Cesium-Seeded High-Current Large Negative Ion Source; Jan. 1997

NIFS-477 H. Kuramoto, K. Toi, N. Haraki, K. Sato, J. Xu, A. Ejiri, K. Narihara, T. Seki, S. Ohdachi, K. Adati, R. Akiyama, Y. Hamada, S. Hirokura, K. Kawahata and M. Kojima,
Study of Toroidal Current Penetration during Current Ramp in JIPP T-IIU with Fast Response Zeeman Polarimeter; Jan. 7, 1997

NIFS-478 H. Sugama and W. Horton,
Neoclassical Electron and Ion Transport in Toroidally Rotating Plasmas; Jan. 1997

NIFS-479 V.L. Vdovin and I.V. Kamenskij,
3D Electromagnetic Theory of ICRF Multi Port Multi Loop Antenna; Jan. 1997

NIFS-480 W.X. Wang, M. Okamoto, N. Nakajima, S Murakami and N. Ohyabu,
Cooling Effect of Secondary Electrons in the High Temperature Divertor Operation; Feb. 1997